Original citation:

LHCb Collaboration (Including: Back, J. J., Dossett, D., Gershon, T. J., Harrison, P. F., Latham, Thomas, Pilar, T., Poluektov, Anton, Reid, M. M., Whitehead, M. and Williams, M. P.). (2012) Measurement of the B s 0-B - s 0 oscillation frequency δm s in B s 0→D s -(3)π decays. Physics Letters B, Volume 709 (Number 3). pp. 177-184.

Permanent WRAP url:

http://wrap.warwick.ac.uk/44735

Physics Letters B 709 (2012) 177–184

Contents lists available at SciVerse ScienceDirect

Physics Letters B

www.elsevier.com/locate/physletb

Measurement of the B_s^0–$\overline{B}_s^0$ oscillation frequency Δm_s in $B_s^0 \to D_s^-(3)\pi$ decays ☆

LHCb Collaboration

ARTICLE INFO

Article history:
Received 21 December 2011
Received in revised form 3 February 2012
Accepted 10 February 2012
Available online 15 February 2012
Editor: W.-D. Schlatter

ABSTRACT

The B_s^0–$\overline{B}_s^0$ oscillation frequency Δm_s is measured with 36 pb^{-1} of data collected in *pp* collisions at $\sqrt{s} = 7$ TeV by the LHCb experiment at the Large Hadron Collider. A total of 1381 $B_s^0 \to D_s^-\pi^+$ and $B_s^0 \to D_s^-\pi^+\pi^-\pi^+$ signal decays are reconstructed, with average decay time resolutions of 44 fs and 36 fs, respectively. An oscillation signal with a statistical significance of 4.6σ is observed. The measured oscillation frequency is $\Delta m_s = 17.63 \pm 0.11\ (\text{stat}) \pm 0.02\ (\text{syst})\ \text{ps}^{-1}$.

1. Introduction

After the observation of B^0–$\overline{B}^0$ mixing and the measurement of its strength in 1987 [1], it took a further 19 years for the B_s^0–$\overline{B}_s^0$ frequency to be measured for the first time [2,3]. This is mainly due to the fact that the B_s^0–$\overline{B}_s^0$ oscillation frequency is 35 times larger than that for the B^0–$\overline{B}^0$ system, posing a considerable challenge for the decay time resolution of detectors. For the LHCb experiment, the ability to resolve these fast B_s^0–$\overline{B}_s^0$ oscillations is a prerequisite for many physics analyses. In particular it is essential for the study of the time-dependent *CP* asymmetry of $B_s^0 \to J/\psi\phi$ decays [4]. The oscillation frequency in the B_s^0–$\overline{B}_s^0$ system is given by the mass difference between the heavy and light mass eigenstates, Δm_s (we use units with $\hbar = 1$). In this Letter, we report a measurement of Δm_s by the LHCb experiment with data collected in 2010.

The LHCb spectrometer covers the pseudo-rapidity range 2 to 5. In this region, *b* hadrons are produced with a large Lorentz boost and have an average flight path of 7 mm. The LHCb detector consists of several components arranged along the LHC beam line. The vertex detector (VELO) surrounds the collision point, followed by a first Ring Imaging Cherenkov (RICH) counter, a tracking station, a dipole magnet, three more tracking stations, a second RICH detector, a calorimeter system and a muon detector. The calorimeter system consists of a scintillating pad detector (SPD), a preshower detector, an electromagnetic calorimeter and a hadronic calorimeter. A detailed description of the detector can be found in Ref. [5]. The precise spatial resolution of the VELO results in an impact parameter resolution of 20–50 μm in the *x* and *y* directions[1] for charged particles with transverse momenta in the range relevant for B_s^0 daughter tracks used in this analysis. The *x* and *y* resolution in the position of the primary vertex reconstruction is about 15 μm while the *z* resolution is about 80 μm. This excellent performance results in the decay time resolution needed to observe the fast B_s^0–$\overline{B}_s^0$ oscillations. The invariant mass resolution provided by the tracking system and the π/K separation given by the two RICH detectors provide clean B_s^0 meson signals with small background. The particle identification capabilities of the RICH together with the calorimeter and muon systems allow the initial flavour of the B_s^0 to be tagged using charged kaons, electrons and muons, respectively.

In the next section, the data sample used and the analysis strategy are introduced. This is followed by descriptions of the analysis of the invariant mass and decay time distributions, and the flavour tagging. Finally, we discuss the fit result for the oscillation frequency and the associated systematic uncertainties.

2. Data sample and analysis strategy

The analysis uses B_s^0 candidates reconstructed in four flavour-specific decay modes,[2] namely $B_s^0 \to D_s^-(\phi(K^+K^-)\pi^-)\pi^+$, $B_s^0 \to D_s^-(K^{*0}(K^+\pi^-)K^-)\pi^+$, $B_s^0 \to D_s^-(K^+K^-\pi^-)\pi^+$ and $B_s^0 \to D_s^-(K^+K^-\pi^-)\pi^+\pi^-\pi^+$. To avoid double counting, candidates that pass the selection criteria of one mode are not considered for the following modes. All reconstructed decays are flavour-specific final states, thus the flavour of the B_s^0 at the time of its decay is given by the charges of the final state particles of the decay. A combination of tagging algorithms is used to identify the B_s^0 flavour at production. The algorithms provide for each event a tagging decision as well as an estimate of the probability that this decision is wrong (mistag probability). These algorithms have been optimized and calibrated using large event samples of flavour-specific $B \to \mu^+D^{*-}X$ and $B^+ \to J/\psi K^+$ decays and a sample of $B^0 \to D^-\pi^+$ decays.

[1] LHCb uses a right-handed Cartesian coordinate system with the *x* direction pointing inside the LHC ring, the *y* direction pointing upwards and the *z* direction running along the beamline from the interaction point towards the spectrometer.

[2] Unless explicitly stated, inclusion of charge-conjugated modes is implied.

0370-2693/ © 2012 CERN. Published by Elsevier B.V. All rights reserved.
doi:10.1016/j.physletb.2012.02.031

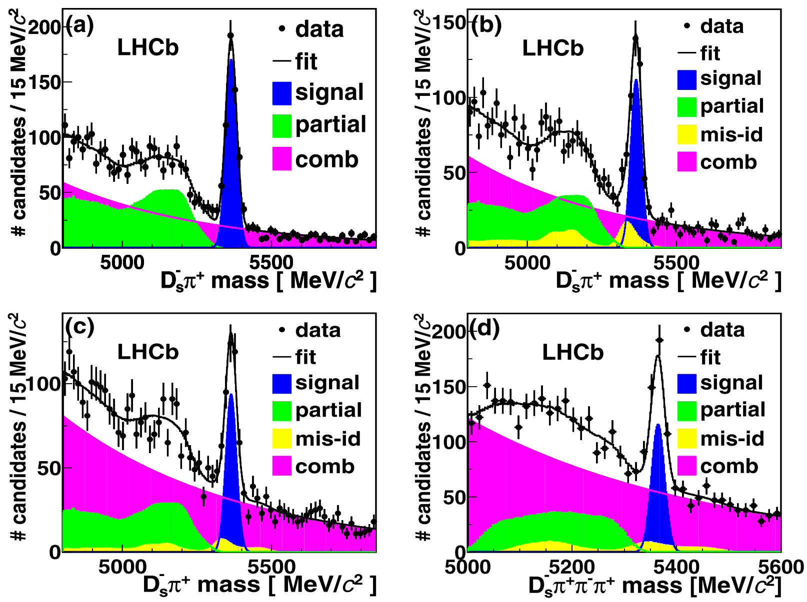

Fig. 1. Mass distributions for (a) $B_s^0 \to D_s^-(\phi\pi^-)\pi^+$, (b) $B_s^0 \to D_s^-(K^{*0}K^-)\pi^+$, (c) $B_s^0 \to D_s^-(K^+K^-\pi^-)\pi^+$ and (d) $B_s^0 \to D_s^-\pi^+\pi^-\pi^+$ candidates. The fits and the various background components are described in the text. "Partial" refers to background from partially reconstructed B_s^0 decays, "mis-id" refers to background from fully or partially reconstructed B^0 and Λ_b decays with one mis-identified daughter particle, and "comb" refers to combinatorial background.

The analysis is based on a data set of 36 pb^{-1} of pp collisions at $\sqrt{s} = 7$ TeV collected in 2010. The first trigger level is implemented in hardware, while the second trigger level is based on software. Trigger conditions were progressively tightened over the duration of the data taking period to cope with the rapidly increasing instantaneous luminosities delivered by the LHC. In the hardware trigger, the events used in this analysis were selected by requiring a cluster with a minimum transverse energy in the hadronic calorimeter. The applied threshold was increased from 2.5 to 3.6 GeV throughout the data taking period. A cut on the number of hits in the SPD detector was applied to reject very high occupancy events. The software trigger for the first 2.4 pb^{-1} of data required a good quality displaced vertex reconstructed from two tracks with transverse momenta p_T of at least 500 MeV/c. For the remaining data, a two-level software trigger was applied. A good quality track with large impact parameter with respect to the primary vertex was required with $p_T > 1.85$ GeV/c and momentum $p > 13.3$ GeV/c [6]. For events passing these criteria, a good quality displaced vertex was required, formed out of two tracks with $p_T > 0.5$ GeV/c and $p > 5$ GeV/c and with a mass variable in the range 2 to 7 GeV/c^2 [7].

Some of the offline event selection criteria are optimized individually for each of the four decay modes under study. In this way specific features such as the masses of the intermediate ϕ and K^{*0} resonances or the helicity angle distribution of the K^{*0} can be used. The selection criteria common to all decay modes exploit the long B_s^0 lifetime by applying cuts on the impact parameters of the daughter tracks, on the angle of the reconstructed B_s^0 momentum relative to the line between the reconstructed primary vertex and the B_s^0 vertex and on the B_s^0 decay time. Additional cuts are applied on the p and p_T of the B_s^0 candidate and its decay products as well as on particle identification variables and on track and vertex quality. Finally, cuts on the impact parameter significance of the reconstructed D_s^- and its distance of closest approach to the primary vertex are applied. The reconstructed D_s^- mass is required to be consistent with the PDG value [8]. After this selection, a total of about 14,400 candidates remain in the $B_s^0 \to D_s^-\pi^+$ invariant mass window of $[4.80, 5.85]$ GeV/c^2 and in the $B_s^0 \to D_s^-\pi^+\pi^-\pi^+$ invariant mass window of $[5.00, 5.60]$ GeV/c^2.

An unbinned likelihood method is employed to fit simultaneously the invariant mass and decay time distributions of the four decay modes. The probability density functions (PDFs) for the signal and for the background in each of the four modes can be written as

$$\mathcal{P} = \mathcal{P}_m(m)\mathcal{P}_t(t, q|\sigma_t, \eta)\mathcal{P}_{\sigma_t}(\sigma_t)\mathcal{P}_\eta(\eta), \tag{1}$$

where m is the reconstructed invariant mass of the B_s^0 candidate, t is its reconstructed decay time and σ_t is the event-by-event estimate of the decay time resolution given by the event reconstruction algorithm. The tagging decision q can be 0 (no tag), -1 (different flavour at production and decay) or $+1$ (same flavour at production and decay). The predicted event-by-event mistag probability η can take values between 0 and 0.5. The terms $\mathcal{P}_m$ and $\mathcal{P}_t$ describe the invariant mass distribution and the decay time distribution, respectively. $\mathcal{P}_t$ is a conditional probability depending on σ_t and η. The terms $\mathcal{P}_{\sigma_t}$ and $\mathcal{P}_\eta$ are required to ensure the proper relative normalization of $\mathcal{P}_t$ for signal and background [9]. These terms are determined directly from the data, using the measured distribution in the upper B_s^0 invariant mass sideband for the background PDF and the sideband subtracted distribution in the invariant mass signal region for the signal PDF.

3. Fit to the invariant mass distributions

The invariant mass of each B_s^0 candidate is determined in a vertex fit using a constraint on the D_s^- mass. The invariant mass spectra for the four decay modes after all selection criteria are shown in Fig. 1. The four distributions are fit simultaneously taking into account contributions from signal, combinatorial background and b decay backgrounds. The signals are described by Gaussian distributions. The fit constrains the mean of the Gaussian distributions to be the same for all four decay modes, whereas it allows the width to be different for the $B_s^0 \to D_s^-\pi^+$ and the $B_s^0 \to D_s^-\pi^+\pi^-\pi^+$ modes, respectively. The combinatorial backgrounds are described by exponential functions. Their parameters are allowed to vary individually for the four decay modes. An alternative parameterization of the combinatorial backgrounds by a first order polynomial is used as part of the systematic studies.

Table 1
B_s^0 signal yields.

Decay mode	Signal yield
$B_s^0 \to D_s^-(\phi\pi^-)\pi^+$	515 ± 25
$B_s^0 \to D_s^-(K^{*0}K^-)\pi^+$	338 ± 27
$B_s^0 \to D_s^-(K^+K^-\pi^-)\pi^+$	283 ± 27
$B_s^0 \to D_s^-\pi^+\pi^-\pi^+$	245 ± 46
Total	1381 ± 65

The b decay backgrounds include partially reconstructed B_s^0 decays, as well as fully and partially reconstructed B^0 and Λ_b decays with one mis-identified daughter particle. Their shapes are derived from a large simulated event sample, where all selection cuts were applied on generator level quantities. The invariant mass spectra were then smeared with a Gaussian distribution to take into account effects of detector resolution. This approach was validated by comparing the results with those from a full simulation including a detailed description of the detector response. The relative normalization factors for the different b decay backgrounds are parameters in the fit. They are constrained to be the same for the three $B_s^0 \to D_s^-\pi^+$ decay modes.

The fit returns a value of $m(B_s^0) = 5364.7 \pm 0.7$ MeV/c^2, about 1.5 MeV/c^2 below the PDG value [8]. This mass shift is attributed to imperfections in the detector alignment and magnetic field calibration. A dedicated study on the momentum scale resulted in a correction for this effect [10]. This calibration procedure is however not used for the analysis presented here as the momentum scale correction largely cancels in the calculation of Δm_s. The mass templates describing b decay backgrounds are shifted according to the observed bias. The fit gives signal mass resolutions of $\sigma_m = 18.1$ MeV/c^2 for the $B_s^0 \to D_s^-\pi^+$ modes and $\sigma_m = 12.7$ MeV/c^2 for the $B_s^0 \to D_s^-\pi^+\pi^-\pi^+$ mode, respectively. The signal yields extracted from the fit are summarized in Table 1. For the remainder of the analysis, the invariant B_s^0 mass range is limited to $[m(B_s^0) - 3\sigma_m, 5.85\ \text{GeV}/c^2]$ and $[m(B_s^0) - 3\sigma_m, 5.60\ \text{GeV}/c^2]$ for the $B_s^0 \to D_s^-\pi^+$ and $B_s^0 \to D_s^-\pi^+\pi^-\pi^+$ modes, respectively. The lower cut of this asymmetric mass window is chosen to reject all background candidates from partial reconstructed B_s^0 decays. The only remaining b decay backgrounds are thus due to mis-identified B^0 and Λ_b decays. The candidates in the high mass sidebands provide a clean sample of combinatorial background. Including them in the fit permits to determine the decay time distribution and tagging behaviour of this background contribution.

The parameters derived in the fit to the mass distributions are fixed for the remainder of the analysis.

4. Fit to the decay time distribution

Ignoring detector resolution effects, selection biases and flavour tagging, the distribution of the decay time t of the signal is described by

$$\mathcal{P}_t(t) \propto \Gamma_s e^{-\Gamma_s t} \cosh\left(\frac{\Delta\Gamma_s}{2} t\right)\theta(t), \tag{2}$$

where Γ_s is the B_s^0 decay width and $\Delta\Gamma_s$ the decay width difference between the heavy and the light mass eigenstates. In the fit $\Delta\Gamma_s$ is fixed to its PDG value of $0.09\Gamma_s$ [8]. As part of the evaluation of systematic uncertainties on Δm_s, the assumed value of $\Delta\Gamma_s$ is varied within its current uncertainty between 0 and $0.2\Gamma_s$. The step function $\theta(t)$ restricts the PDF to positive decay times.

The true decay time is convolved with the decay time resolution function of the detector. An event-by-event estimate of the decay time resolution is calculated by the fitting algorithm, which reconstructs the decay vertex of the B_s^0 and computes its decay length and decay time. No constraint on the D_s^- mass is applied in the computation of the decay time in order to minimize sensitivity to the knowledge of the momentum scale of the experiment. The decay time uncertainty calculated by the fitting algorithm does not include possible effects from an imperfect understanding of the detector material or its spatial alignment. To correct for such effects, the calculated event-by-event decay time uncertainties, σ_t, are multiplied by a constant scale factor S_{σ_t}. The value of S_{σ_t} is determined from data, using a sample of fake B_s^0 candidates formed by a prompt D_s^- and a π^+ from the primary vertex. The contamination due to secondary D_s^- from B decays is estimated and statistically subtracted using the measured D_s^- impact parameter distribution. The distribution of decay times for this fake B_s^0 sample, each divided by its calculated event-by-event uncertainty, is fitted with a Gaussian function and S_{σ_t} is taken as the resulting standard deviation. Using the full sample of fake B_s^0 candidates, a value of $S_{\sigma_t} = 1.3$ is obtained. This value is used as the nominal scale factor in the Δm_s analysis. Studying different regions of phase space of the fake B_s^0 candidates separately, values for S_{σ_t} between 1.2 and 1.4 are obtained. This variation is taken into account for evaluating the systematic uncertainties on Δm_s. Including the nominal scale factor $S_{\sigma_t} = 1.3$, the average decay time resolution is 44 fs for the $B_s^0 \to D_s^-\pi^+$ sample and 36 fs for the $B_s^0 \to D_s^-\pi^+\pi^-\pi^+$ sample. The decay time resolution is taken into account in the PDF by convolving Eq. (2) with a Gaussian G with mean zero and standard deviation $1.3\sigma_t$.

The shape of the decay time distribution is distorted by trigger and offline selection criteria which require several particles with large impact parameter with respect to the primary vertex. This is accounted for in the PDF by introducing an acceptance function $\epsilon(t)$, derived from a full detector simulation. Determining $\epsilon(t)$ from simulation is deemed acceptable since it cancels to first order in the determination of Δm_s. The untagged signal decay time PDF becomes

$$\mathcal{P}_t(t|\sigma_t) \propto \left[\Gamma_s e^{-\Gamma_s t} \cosh\left(\frac{\Delta\Gamma_s}{2} t\right)\theta(t)\right] \otimes G(t, S_{\sigma_t}\sigma_t)\epsilon(t). \tag{3}$$

The decay time distributions for the b decay backgrounds from B^0 and Λ_b decays are described in the same way as that for signal B_s^0 candidates, using the PDG values for their lifetimes and $\Delta\Gamma = 0$. The shape of the decay time distribution for the combinatorial background is described by the sum of two exponential functions multiplied by a second order polynomial. The parameters of these functions are derived from the high mass sidebands. Fig. 2 illustrates the results of the lifetime fit. Within its statistical uncertainty the reconstructed B_s^0 lifetime agrees with the PDG value [8].

5. Flavour tagging

To determine the flavour of the B_s^0 candidate at production we exploit the fact that b quarks are predominantly produced in quark–antiquark pairs. The quark which is not part of the B_s^0 meson gives rise to an opposite-side b hadron. For opposite-side b hadron decay candidates, the charge of displaced muons, electrons and kaons and a decay vertex charge estimate are combined using a neural network to form a single opposite-side tagging decision. The tagging decision has a probability to be wrong which is called the mistag probability, ω. For each event an estimate, η, of the mistag probability, is determined based upon topological and kinematic properties of the event, including the number of primary vertices, the number of tagging particle candidates, the impact parameter of the tagging particle and of the B_s^0 candidate with respect to the primary vertex, and the p and p_{T} of the selected

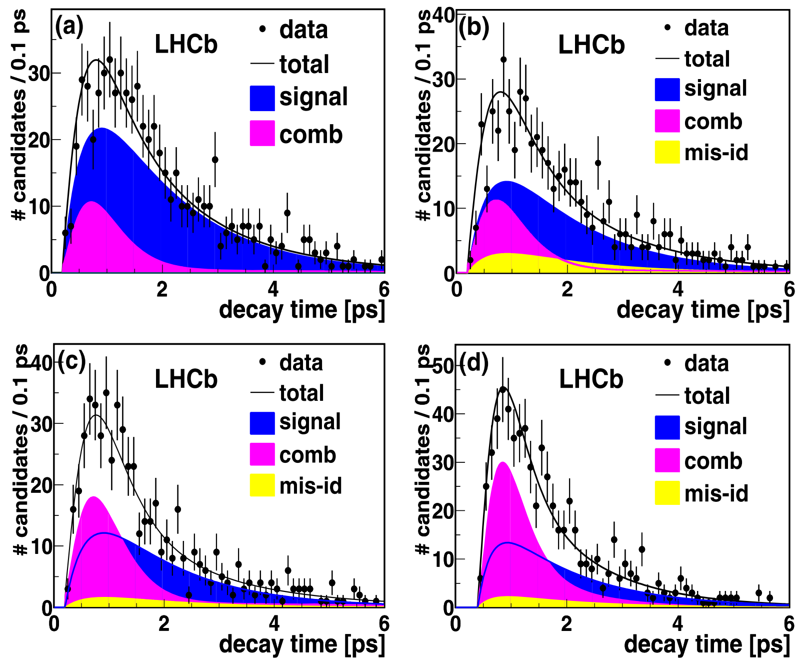

Fig. 2. Decay time distributions for (a) $B_s^0 \to D_s^-(\phi\pi^-)\pi^+$, (b) $B_s^0 \to D_s^-(K^{*0}K^-)\pi^+$, (c) $B_s^0 \to D_s^-(K^+K^-\pi^-)\pi^+$ and (d) $B_s^0 \to D_s^-\pi^+\pi^-\pi^+$ candidates. The data and the fit projection are from a mass range of $\pm\, 3\sigma_m$ around the reconstructed B_s^0 mass. The abbreviations for the various fit components are introduced in Fig. 1.

tagging particle and the B_s^0 candidate. The optimization of the tagging algorithms and an initial calibration of η are performed in an independent analysis using large event samples of $B \to \mu^+ D^{*-} X$ and $B^+ \to J/\psi K^+$ decays. More details on the individual tagging algorithms and this calibration procedure can be found in Ref. [11].

The $B \to \mu^+ D^{*-} X$ and $B^+ \to J/\psi K^+$ events used in the optimization and calibration were collected using different trigger and selection criteria than for the $B_s^0 \to D_s^-\pi^+$ and $B_s^0 \to D_s^-\pi^+\pi^-\pi^+$ events used in the Δm_s analysis described here. As trigger and selection cuts can bias the distributions of the event properties used by the tagging algorithms, this could result in a biased estimate for the $B_s^0 \to D_s^-\pi^+$ and $B_s^0 \to D_s^-\pi^+\pi^-\pi^+$ events. Therefore, a re-calibration is performed using a sample of 6000 $B^0 \to D^-\pi^+$ events, which have a similar topology to the $B_s^0 \to D_s^-\pi^+$ and $B_s^0 \to D_s^-\pi^+\pi^-\pi^+$ events, and were collected using the same trigger and similar selection cuts. This event sample is used to perform a measurement of the B^0–$\overline{B}^0$ flavour oscillation using a very similar method to that described here. In that measurement the true event mistag probability, ω, is parameterized as a linear function of η using the relationship $\omega(\eta) = a + b \times (\eta - \langle\eta\rangle)$, where $\langle\eta\rangle = 0.3276$ is the mean of the distribution of the η values obtained from the initial tagger optimization. The parameters $a = 0.311 \pm 0.022$ and $b = 0.61 \pm 0.25$ are determined as part of the maximum likelihood fit of the B^0–$\overline{B}^0$ oscillation signal and found to be consistent with the original calibration. As a by-product of this re-calibration procedure the B^0–$\overline{B}^0$ oscillation frequency is measured. The resulting value of $\Delta m_d = 0.499 \pm 0.032\ \text{(stat)} \pm 0.003\ \text{(syst)}\ \text{ps}^{-1}$, though statistically less precise, is in good agreement with the PDG value of $\Delta m_d = 0.507 \pm 0.004\ \text{ps}^{-1}$ [8] and provides a valuable cross check of the procedure.

The statistical power of the tagging is determined by the "effective" tagging efficiency for signal events and is defined as

$$\epsilon_{\text{eff}} = \epsilon_s \times \frac{1}{\sum_i W_i} \sum_i \bigl(1 - 2\omega(\eta_i)\bigr)^2 \times W_i, \tag{4}$$

where the signal tagging efficiency ϵ_s is a free parameter in the fit of the oscillation frequency described in the next section. W_i is the probability for being a signal event as determined by the invariant mass and decay time PDFs. The index i runs over all B_s^0 candidates.

6. Measurement of the oscillation frequency

To determine the oscillation frequency, Δm_s, the decay time PDF for signal candidates with tagging information is modified in the following way:

$$\begin{aligned}\mathcal{P}_t(t, q|\sigma_t, \eta) \propto \Biggl\{ &\Gamma_s e^{-\Gamma_s t} \frac{1}{2} \Biggl[\cosh\left(\frac{\Delta\Gamma_s}{2} t\right) \\ &+ q\bigl[1 - 2\omega(\eta)\bigr] \cos(\Delta m_s t) \Biggr] \theta(t) \Biggr\} \\ &\otimes G(t, S_{\sigma_t}\sigma_t)\epsilon(t)\epsilon_s.\end{aligned} \tag{5}$$

The decay time PDF for untagged signal events is given by Eq. (3) multiplied by an additional factor $(1 - \epsilon_s)$. The calibration parameters a and b of the mistag probability $\omega(\eta)$ are identical for all signal and b decay background components. Within Gaussian constraints they are set to the values found in the calibration described in the previous section. The signal tagging efficiency ϵ_s for the $B_s^0 \to D_s^-\pi^+$ and $B_s^0 \to D_s^-\pi^+\pi^-\pi^+$ modes are two separate parameters in the fit. The same values of ϵ_s are however used for signal and b decay background components in each of these two categories. In the description of the combinatorial background a separate parameter for the tagging efficiency is introduced for each of the four modes. In addition, tagging asymmetry parameters are introduced in the PDFs for the combinatorial background, to allow for a different number of events tagged as B_s^0 or $\overline{B}_s^0$ in each mode. As expected the fit results for these asymmetries are compatible with zero.

The fit for the oscillation frequency Δm_s is performed simultaneously to all four B_s^0 decay modes and gives $\Delta m_s = 17.63 \pm$

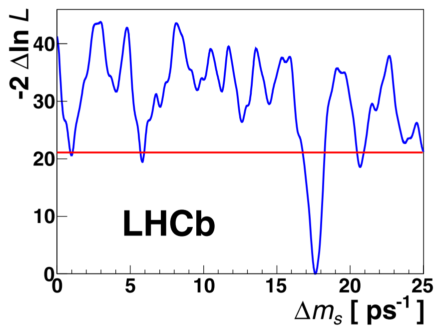

Fig. 3. Likelihood scan for Δm_s in the range [0.0, 25.0] ps^{-1}. The line at $-2\Delta \ln L = 20.9$ indicates the value in the limit $\Delta m_s = \infty$.

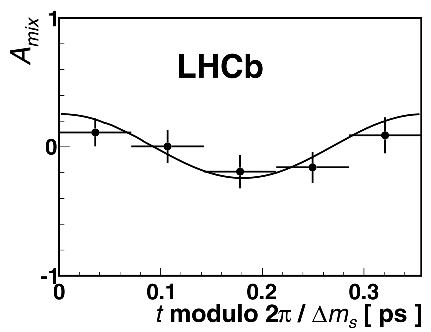

Fig. 4. Measured asymmetry for B_s^0 candidates in bins of the decay time t modulo $2\pi/\Delta m_s$. The projection of the likelihood fit is superimposed.

0.11 ps^{-1} (statistical uncertainty only). Signal tagging efficiencies of $\epsilon_s = (23.6 \pm 1.3)\%$ and $\epsilon_s = (17.6 \pm 3.2)\%$ are found for the $B_s^0 \to D_s^-\pi^+$ and $B_s^0 \to D_s^-\pi^+\pi^-\pi^+$ modes, respectively. The combined effective tagging efficiency for all four modes is $\epsilon_{\text{eff}} = (3.8 \pm 2.1)\%$. The likelihood profile as a function of the assumed oscillation frequency Δm_s is shown in Fig. 3. The statistical significance of the signal is evaluated to be 4.6σ by comparing the likelihood value at the minimum of the fit with that found in the limit $\Delta m_s = \infty$.

To illustrate the oscillation pattern, we define the time-dependent mixing asymmetry as

$$A_{\text{mix}}(t) = \frac{N^+(t) - N^-(t)}{N^+(t) + N^-(t)} \tag{6}$$

where $N^+(t)$ and $N^-(t)$ are the number of background subtracted B_s^0 signal candidates with a given decay time t and tagging decision $+1$ and -1, respectively. Note, that this definition of the asymmetry does not include any information on the mistag probabilities and therefore does not use the full information of the likelihood fit. Despite the limited size of the sample, the oscillation pattern is clearly visible when the asymmetry is plotted in bins of the decay time modulo $2\pi/\Delta m_s$ (Fig. 4). In an ideal scenario of perfect tagging and perfect decay time resolution the amplitude of this oscillation would be 1.0. The observed amplitude is reduced due to the performance of the tagging algorithm by a factor 0.41. Another reduction of 0.65 occurs due to the limited decay time resolution.

7. Systematic uncertainties

The dominant source of systematic uncertainty is due to the knowledge of the absolute decay time scale of the experiment. This uncertainty is dominated by the knowledge of the z scale. A relative uncertainty of 0.1% on the z scale and thus on the decay length is assigned based on comparisons of detector surveys and

Table 2
Summary of the systematic uncertainties on Δm_s. The total systematic uncertainty is defined as the quadratic sum of the individual components.

Source	Uncertainty [ps^{-1}]
Momentum scale	0.004
z scale	0.018
Combinatorial background mass shape	0.010
Decay time resolution	0.006
Total systematic uncertainty	0.022

a software alignment using reconstructed tracks. This leads to a systematic uncertainty of 0.018 ps^{-1} on Δm_s. A second contribution to the decay time scale is due to the momentum scale of the experiment. From an independent analysis of the mass scale using various known resonances an uncertainty of the uncalibrated momentum scale of less than 0.1% is estimated. This uncertainty partially cancels as it enters both the reconstructed B_s^0 mass and the B_s^0 momentum. The resulting relative uncertainty on the decay time is 0.02%, which translates to an absolute systematic uncertainty of 0.004 ps^{-1} on Δm_s.

The next largest systematic uncertainty is related to the description of the combinatorial background in the fit to the mass spectra. It is evaluated by replacing the exponential function by a first order polynomial. Based on the shift in the value obtained for Δm_s, a systematic uncertainty of 0.010 ps^{-1} is assigned. Finally, based on variations of the decay time resolution scale factor S_{σ_t} within its estimated uncertainty from 1.2 to 1.4, a systematic uncertainty of 0.006 ps^{-1} is assigned on Δm_s. These contributions to the systematic uncertainty on Δm_s are summarized in Table 2.

Various other possible sources of systematic effects have been studied, such as the decay time resolution model, the decay time acceptance, releasing parameters of the invariant mass and decay time PDF in the mixing fit, different parameterizations of the invariant mass of the b decay backgrounds and variations of the value of $\Delta\Gamma_s$. They are found to be negligible.

8. Conclusion

A measurement of the B_s^0–$\bar{B}_s^0$ oscillation frequency Δm_s is performed using $B_s^0 \to D_s^-\pi^+$ and $B_s^0 \to D_s^-\pi^+\pi^-\pi^+$ decays collected in 36 pb^{-1} of pp collisions at $\sqrt{s} = 7$ TeV in 2010. The result is found to be

$$\Delta m_s = 17.63 \pm 0.11\ (\text{stat}) \pm 0.02\ (\text{syst})\ \text{ps}^{-1}. \tag{7}$$

This is in good agreement with the previous best measurement of $\Delta m_s = 17.77 \pm 0.10$ (stat) ± 0.07 (syst) ps^{-1}, reported by the CDF Collaboration [3]. As a by product of the analysis we also determine a value for the B^0–B^0 oscillation frequency $\Delta m_d = 0.499 \pm 0.032$ (stat) ± 0.003 (syst) ps^{-1}. Our results are completely dominated by statistical uncertainties and thus significant improvements are expected with larger data sets.

Acknowledgements

We express our gratitude to our colleagues in the CERN accelerator departments for the excellent performance of the LHC. We thank the technical and administrative staff at CERN and at the LHCb institutes, and acknowledge support from the National Agencies: CAPES, CNPq, FAPERJ and FINEP (Brazil); CERN; NSFC (China); CNRS/IN2P3 (France); BMBF, DFG, HGF and MPG (Germany); SFI (Ireland); INFN (Italy); FOM and NWO (The Netherlands); SCSR (Poland); ANCS (Romania); MinES of Russia and Rosatom (Russia); MICINN, XuntaGal and GENCAT (Spain); SNSF and SER (Switzerland); NAS Ukraine (Ukraine); STFC (United Kingdom); NSF (USA).

We also acknowledge the support received from the ERC under FP7 and the Region Auvergne.

Open access

References

[1] ARGUS Collaboration, H. Albrecht, et al., Phys. Lett. B 192 (1987) 245.
[2] D0 Collaboration, V.M. Abazov, et al., Phys. Rev. Lett. 97 (2006) 021802.
[3] CDF Collaboration, A. Abulencia, et al., Phys. Rev. Lett. 97 (2006) 062003.
[4] LHCb Collaboration, R. Aaij, et al., Measurement of the CP-violating phase ϕ_s in the decay $B_s^0 \to J/\psi\phi$, Phys. Rev. Lett., in press, arXiv:1112.3183.
[5] LHCb Collaboration, A.A. Alves Jr., et al., JINST 3 (2008) S08005.
[6] V.V. Gligorov, A single track HLT1 trigger, LHCb-PUB-2011-003.
[7] M. Williams, et al., The HLT2 topological lines, LHCb-PUB-2011-002.
[8] Particle Data Group, K. Nakamura, et al., J. Phys. G 37 (2010) 075021.
[9] G. Punzi, Comments on likelihood fits with variable resolution, eConf C030908 WELT002, 2003.
[10] LHCb Collaboration, Measurement of b hadron masses with exclusive $J/\psi X$ decays in 2010 data, LHCb-CONF-2011-027.
[11] LHCb Collaboration, Optimization and calibration of the LHCb flavour tagging performance using 2010 data, LHCb-CONF-2011-003;
LHCb Collaboration, R. Aaij, et al., Flavour tagging of B mesons at LHCb, in preparation; to be submitted to Eur. J. Phys. C, LHCb-PAPER-2011-027.

LHCb Collaboration

R. Aaij [23], B. Adeva [36], M. Adinolfi [42], C. Adrover [6], A. Affolder [48], Z. Ajaltouni [5], J. Albrecht [37], F. Alessio [37], M. Alexander [47], G. Alkhazov [29], P. Alvarez Cartelle [36], A.A. Alves Jr. [22], S. Amato [2], Y. Amhis [38], J. Anderson [39], R.B. Appleby [50], O. Aquines Gutierrez [10], F. Archilli [18,37], L. Arrabito [53], A. Artamonov [34], M. Artuso [52,37], E. Aslanides [6], G. Auriemma [22,m], S. Bachmann [11], J.J. Back [44], D.S. Bailey [50], V. Balagura [30,37], W. Baldini [16], R.J. Barlow [50], C. Barschel [37], S. Barsuk [7], W. Barter [43], A. Bates [47], C. Bauer [10], Th. Bauer [23], A. Bay [38], I. Bediaga [1], K. Belous [34], I. Belyaev [30,37], E. Ben-Haim [8], M. Benayoun [8], G. Bencivenni [18], S. Benson [46], J. Benton [42], R. Bernet [39], M.-O. Bettler [17], M. van Beuzekom [23], A. Bien [11], S. Bifani [12], A. Bizzeti [17,h], P.M. Bjørnstad [50], T. Blake [49], F. Blanc [38], C. Blanks [49], J. Blouw [11], S. Blusk [52], A. Bobrov [33], V. Bocci [22], A. Bondar [33], N. Bondar [29], W. Bonivento [15], S. Borghi [47], A. Borgia [52], T.J.V. Bowcock [48], C. Bozzi [16], T. Brambach [9], J. van den Brand [24], J. Bressieux [38], D. Brett [50], S. Brisbane [51], M. Britsch [10], T. Britton [52], N.H. Brook [42], H. Brown [48], A. Büchler-Germann [39], I. Burducea [28], A. Bursche [39], J. Buytaert [37], S. Cadeddu [15], J.M. Caicedo Carvajal [37], O. Callot [7], M. Calvi [20,j], M. Calvo Gomez [35,n], A. Camboni [35], P. Campana [18,37], A. Carbone [14], G. Carboni [21,k], R. Cardinale [19,37,i], A. Cardini [15], L. Carson [36], K. Carvalho Akiba [23], G. Casse [48], M. Cattaneo [37], M. Charles [51], Ph. Charpentier [37], N. Chiapolini [39], K. Ciba [37], X. Cid Vidal [36], G. Ciezarek [49], P.E.L. Clarke [46,37], M. Clemencic [37], H.V. Cliff [43], J. Closier [37], C. Coca [28], V. Coco [23], J. Cogan [6], P. Collins [37], F. Constantin [28], G. Conti [38], A. Contu [51], A. Cook [42], M. Coombes [42], G. Corti [37], G.A. Cowan [38], R. Currie [46], B. D'Almagne [7], C. D'Ambrosio [37], P. David [8], I. De Bonis [4], S. De Capua [21,k], M. De Cian [39], F. De Lorenzi [12], J.M. De Miranda [1], L. De Paula [2], P. De Simone [18], D. Decamp [4], M. Deckenhoff [9], H. Degaudenzi [38,37], M. Deissenroth [11], L. Del Buono [8], C. Deplano [15], O. Deschamps [5], F. Dettori [15,d], J. Dickens [43], H. Dijkstra [37], P. Diniz Batista [1], S. Donleavy [48], A. Dosil Suárez [36], D. Dossett [44], A. Dovbnya [40], F. Dupertuis [38], R. Dzhelyadin [34], C. Eames [49], S. Easo [45], U. Egede [49], V. Egorychev [30], S. Eidelman [33], D. van Eijk [23], F. Eisele [11], S. Eisenhardt [46], R. Ekelhof [9], L. Eklund [47], Ch. Elsasser [39], D.G. d'Enterria [35,o], D. Esperante Pereira [36], L. Estève [43], A. Falabella [16,e], E. Fanchini [20,j], C. Färber [11], G. Fardell [46], C. Farinelli [23], S. Farry [12], V. Fave [38], V. Fernandez Albor [36], M. Ferro-Luzzi [37], S. Filippov [32], C. Fitzpatrick [46], M. Fontana [10], F. Fontanelli [19,i], R. Forty [37], M. Frank [37], C. Frei [37], M. Frosini [17,37,f], S. Furcas [20], A. Gallas Torreira [36], D. Galli [14,c], M. Gandelman [2], P. Gandini [51], Y. Gao [3], J.-C. Garnier [37], J. Garofoli [52], J. Garra Tico [43], L. Garrido [35], C. Gaspar [37], N. Gauvin [38], M. Gersabeck [37], T. Gershon [44,37], Ph. Ghez [4], V. Gibson [43], V.V. Gligorov [37], C. Göbel [54], D. Golubkov [30], A. Golutvin [49,30,37], A. Gomes [2], H. Gordon [51], M. Grabalosa Gándara [35], R. Graciani Diaz [35], L.A. Granado Cardoso [37], E. Graugés [35], G. Graziani [17], A. Grecu [28], S. Gregson [43], B. Gui [52], E. Gushchin [32], Yu. Guz [34], T. Gys [37], G. Haefeli [38], C. Haen [37], S.C. Haines [43], T. Hampson [42], S. Hansmann-Menzemer [11,*], R. Harji [49], N. Harnew [51], J. Harrison [50], P.F. Harrison [44], J. He [7], V. Heijne [23], K. Hennessy [48], P. Henrard [5], J.A. Hernando Morata [36], E. van Herwijnen [37], E. Hicks [48], W. Hofmann [10], K. Holubyev [11], P. Hopchev [4], W. Hulsbergen [23], P. Hunt [51], T. Huse [48], R.S. Huston [12], D. Hutchcroft [48], D. Hynds [47], V. Iakovenko [41], P. Ilten [12], J. Imong [42], R. Jacobsson [37], A. Jaeger [11], M. Jahjah Hussein [5], E. Jans [23], F. Jansen [23], P. Jaton [38], B. Jean-Marie [7], F. Jing [3], M. John [51], D. Johnson [51], C.R. Jones [43], B. Jost [37], S. Kandybei [40], M. Karacson [37], T.M. Karbach [9], J. Keaveney [12], U. Kerzel [37], T. Ketel [24], A. Keune [38], B. Khanji [6], Y.M. Kim [46], M. Knecht [38], S. Koblitz [37],

P. Koppenburg [23], A. Kozlinskiy [23], L. Kravchuk [32], K. Kreplin [11], M. Kreps [44], G. Krocker [11], P. Krokovny [11], F. Kruse [9], K. Kruzelecki [37], M. Kucharczyk [20,25,37], S. Kukulak [25], R. Kumar [14,37], T. Kvaratskheliya [30,37], V.N. La Thi [38], D. Lacarrere [37], G. Lafferty [50], A. Lai [15], D. Lambert [46], R.W. Lambert [37], E. Lanciotti [37], G. Lanfranchi [18], C. Langenbruch [11], T. Latham [44], R. Le Gac [6], J. van Leerdam [23], J.-P. Lees [4], R. Lefèvre [5], A. Leflat [31,37], J. Lefrançois [7], O. Leroy [6], T. Lesiak [25], L. Li [3], L. Li Gioi [5], M. Lieng [9], M. Liles [48], R. Lindner [37], C. Linn [11], B. Liu [3], G. Liu [37], J.H. Lopes [2], E. Lopez Asamar [35], N. Lopez-March [38], J. Luisier [38], F. Machefert [7], I.V. Machikhiliyan [4,30], F. Maciuc [10], O. Maev [29,37], J. Magnin [1], S. Malde [51], R.M.D. Mamunur [37], G. Manca [15,d], G. Mancinelli [6], N. Mangiafave [43], U. Marconi [14], R. Märki [38], J. Marks [11], G. Martellotti [22], A. Martens [7], L. Martin [51], A. Martín Sánchez [7], D. Martinez Santos [37], A. Massafferri [1], Z. Mathe [12], C. Matteuzzi [20], M. Matveev [29], E. Maurice [6], B. Maynard [52], A. Mazurov [32,16,37], G. McGregor [50], R. McNulty [12], C. Mclean [14], M. Meissner [11], M. Merk [23], J. Merkel [9], R. Messi [21,k], S. Miglioranzi [37], D.A. Milanes [13,37], M.-N. Minard [4], S. Monteil [5], D. Moran [12], P. Morawski [25], R. Mountain [52], I. Mous [23], F. Muheim [46], K. Müller [39], R. Muresan [28,38], B. Muryn [26], M. Musy [35], J. Mylroie-Smith [48], P. Naik [42], T. Nakada [38], R. Nandakumar [45], J. Nardulli [45], I. Nasteva [1], M. Nedos [9], M. Needham [46], N. Neufeld [37], C. Nguyen-Mau [38,p], M. Nicol [7], S. Nies [9], V. Niess [5], N. Nikitin [31], A. Oblakowska-Mucha [26], V. Obraztsov [34], S. Oggero [23], S. Ogilvy [47], O. Okhrimenko [41], R. Oldeman [15,d], M. Orlandea [28], J.M. Otalora Goicochea [2], P. Owen [49], B. Pal [52], J. Palacios [39], M. Palutan [18], J. Panman [37], A. Papanestis [45], M. Pappagallo [13,b], C. Parkes [47,37], C.J. Parkinson [49], G. Passaleva [17], G.D. Patel [48], M. Patel [49], S.K. Paterson [49], G.N. Patrick [45], C. Patrignani [19,i], C. Pavel-Nicorescu [28], A. Pazos Alvarez [36], A. Pellegrino [23], G. Penso [22,l], M. Pepe Altarelli [37], S. Perazzini [14,c], D.L. Perego [20,j], E. Perez Trigo [36], A. Pérez-Calero Yzquierdo [35], P. Perret [5], M. Perrin-Terrin [6], G. Pessina [20], A. Petrella [16,37], A. Petrolini [19,i], B. Pie Valls [35], B. Pietrzyk [4], T. Pilar [44], D. Pinci [22], R. Plackett [47], S. Playfer [46], M. Plo Casasus [36], G. Polok [25], A. Poluektov [44,33], E. Polycarpo [2], D. Popov [10], B. Popovici [28], C. Potterat [35], A. Powell [51], T. du Pree [23], J. Prisciandaro [38], V. Pugatch [41], A. Puig Navarro [35], W. Qian [52], J.H. Rademacker [42], B. Rakotomiaramanana [38], M.S. Rangel [2], I. Raniuk [40], G. Raven [24], S. Redford [51], M.M. Reid [44], A.C. dos Reis [1], S. Ricciardi [45], K. Rinnert [48], D.A. Roa Romero [5], P. Robbe [7], E. Rodrigues [47], F. Rodrigues [2], P. Rodriguez Perez [36], G.J. Rogers [43], S. Roiser [37], V. Romanovsky [34], J. Rouvinet [38], T. Ruf [37], H. Ruiz [35], G. Sabatino [21,k], J.J. Saborido Silva [36], N. Sagidova [29], P. Sail [47], B. Saitta [15,d], C. Salzmann [39], M. Sannino [19,i], R. Santacesaria [22], R. Santinelli [37], E. Santovetti [21,k], M. Sapunov [6], A. Sarti [18,l], C. Satriano [22,m], A. Satta [21], M. Savrie [16,e], D. Savrina [30], P. Schaack [49], M. Schiller [11], S. Schleich [9], M. Schmelling [10], B. Schmidt [37], O. Schneider [38], A. Schopper [37], M.-H. Schune [7], R. Schwemmer [37], A. Sciubba [18,l], M. Seco [36], A. Semennikov [30], K. Senderowska [26], I. Sepp [49], N. Serra [39], J. Serrano [6], P. Seyfert [11], B. Shao [3], M. Shapkin [34], I. Shapoval [40,37], P. Shatalov [30], Y. Shcheglov [29], T. Shears [48], L. Shekhtman [33], O. Shevchenko [40], V. Shevchenko [30], A. Shires [49], R. Silva Coutinho [54], H.P. Skottowe [43], T. Skwarnicki [52], A.C. Smith [37], N.A. Smith [48], K. Sobczak [5], F.J.P. Soler [47], A. Solomin [42], F. Soomro [49], B. Souza De Paula [2], B. Spaan [9], A. Sparkes [46], P. Spradlin [47], F. Stagni [37], S. Stahl [11], O. Steinkamp [39], S. Stoica [28], S. Stone [52,37], B. Storaci [23], M. Straticiuc [28], U. Straumann [39], N. Styles [46], V.K. Subbiah [37], S. Swientek [9], M. Szczekowski [27], P. Szczypka [38], T. Szumlak [26], S. T'Jampens [4], E. Teodorescu [28], F. Teubert [37], C. Thomas [51,45], E. Thomas [37], J. van Tilburg [11], V. Tisserand [4], M. Tobin [39], S. Topp-Joergensen [51], M.T. Tran [38], A. Tsaregorodtsev [6], N. Tuning [23], A. Ukleja [27], P. Urquijo [52], U. Uwer [11], V. Vagnoni [14], G. Valenti [14], R. Vazquez Gomez [35], P. Vazquez Regueiro [36], S. Vecchi [16], J.J. Velthuis [42], M. Veltri [17,g], K. Vervink [37], B. Viaud [7], I. Videau [7], X. Vilasis-Cardona [35,n], J. Visniakov [36], A. Vollhardt [39], D. Voong [42], A. Vorobyev [29], H. Voss [10], K. Wacker [9], S. Wandernoth [11], J. Wang [52], D.R. Ward [43], A.D. Webber [50], D. Websdale [49], M. Whitehead [44], D. Wiedner [11], L. Wiggers [23], G. Wilkinson [51], M.P. Williams [44,45], M. Williams [49], F.F. Wilson [45], J. Wishahi [9], M. Witek [25,37], W. Witzeling [37], S.A. Wotton [43], K. Wyllie [37], Y. Xie [46], F. Xing [51], Z. Yang [3], R. Young [46], O. Yushchenko [34], M. Zavertyaev [10,a], L. Zhang [52], W.C. Zhang [12], Y. Zhang [3], A. Zhelezov [11], L. Zhong [3], E. Zverev [31], A. Zvyagin [37]

[1] *Centro Brasileiro de Pesquisas Físicas (CBPF), Rio de Janeiro, Brazil*
[2] *Universidade Federal do Rio de Janeiro (UFRJ), Rio de Janeiro, Brazil*
[3] *Center for High Energy Physics, Tsinghua University, Beijing, China*
[4] *LAPP, Université de Savoie, CNRS/IN2P3, Annecy-Le-Vieux, France*
[5] *Clermont Université, Université Blaise Pascal, CNRS/IN2P3, LPC, Clermont-Ferrand, France*
[6] *CPPM, Aix-Marseille Université, CNRS/IN2P3, Marseille, France*

[7] *LAL, Université Paris-Sud, CNRS/IN2P3, Orsay, France*
[8] *LPNHE, Université Pierre et Marie Curie, Université Paris Diderot, CNRS/IN2P3, Paris, France*
[9] *Fakultät Physik, Technische Universität Dortmund, Dortmund, Germany*
[10] *Max-Planck-Institut für Kernphysik (MPIK), Heidelberg, Germany*
[11] *Physikalisches Institut, Ruprecht-Karls-Universität Heidelberg, Heidelberg, Germany*
[12] *School of Physics, University College Dublin, Dublin, Ireland*
[13] *Sezione INFN di Bari, Bari, Italy*
[14] *Sezione INFN di Bologna, Bologna, Italy*
[15] *Sezione INFN di Cagliari, Cagliari, Italy*
[16] *Sezione INFN di Ferrara, Ferrara, Italy*
[17] *Sezione INFN di Firenze, Firenze, Italy*
[18] *Laboratori Nazionali dell'INFN di Frascati, Frascati, Italy*
[19] *Sezione INFN di Genova, Genova, Italy*
[20] *Sezione INFN di Milano Bicocca, Milano, Italy*
[21] *Sezione INFN di Roma Tor Vergata, Roma, Italy*
[22] *Sezione INFN di Roma La Sapienza, Roma, Italy*
[23] *Nikhef National Institute for Subatomic Physics, Amsterdam, Netherlands*
[24] *Nikhef National Institute for Subatomic Physics and Vrije Universiteit, Amsterdam, Netherlands*
[25] *Henryk Niewodniczanski Institute of Nuclear Physics, Polish Academy of Sciences, Cracow, Poland*
[26] *Faculty of Physics & Applied Computer Science, Cracow, Poland*
[27] *Soltan Institute for Nuclear Studies, Warsaw, Poland*
[28] *Horia Hulubei National Institute of Physics and Nuclear Engineering, Bucharest-Magurele, Romania*
[29] *Petersburg Nuclear Physics Institute (PNPI), Gatchina, Russia*
[30] *Institute of Theoretical and Experimental Physics (ITEP), Moscow, Russia*
[31] *Institute of Nuclear Physics, Moscow State University (SINP MSU), Moscow, Russia*
[32] *Institute for Nuclear Research of the Russian Academy of Sciences (INR RAN), Moscow, Russia*
[33] *Budker Institute of Nuclear Physics (SB RAS) and Novosibirsk State University, Novosibirsk, Russia*
[34] *Institute for High Energy Physics (IHEP), Protvino, Russia*
[35] *Universitat de Barcelona, Barcelona, Spain*
[36] *Universidad de Santiago de Compostela, Santiago de Compostela, Spain*
[37] *European Organization for Nuclear Research (CERN), Geneva, Switzerland*
[38] *Ecole Polytechnique Fédérale de Lausanne (EPFL), Lausanne, Switzerland*
[39] *Physik-Institut, Universität Zürich, Zürich, Switzerland*
[40] *NSC Kharkiv Institute of Physics and Technology (NSC KIPT), Kharkiv, Ukraine*
[41] *Institute for Nuclear Research of the National Academy of Sciences (KINR), Kyiv, Ukraine*
[42] *H.H. Wills Physics Laboratory, University of Bristol, Bristol, United Kingdom*
[43] *Cavendish Laboratory, University of Cambridge, Cambridge, United Kingdom*
[44] *Department of Physics, University of Warwick, Coventry, United Kingdom*
[45] *STFC Rutherford Appleton Laboratory, Didcot, United Kingdom*
[46] *School of Physics and Astronomy, University of Edinburgh, Edinburgh, United Kingdom*
[47] *School of Physics and Astronomy, University of Glasgow, Glasgow, United Kingdom*
[48] *Oliver Lodge Laboratory, University of Liverpool, Liverpool, United Kingdom*
[49] *Imperial College London, London, United Kingdom*
[50] *School of Physics and Astronomy, University of Manchester, Manchester, United Kingdom*
[51] *Department of Physics, University of Oxford, Oxford, United Kingdom*
[52] *Syracuse University, Syracuse, NY, United States*
[53] *CC-IN2P3, CNRS/IN2P3, Lyon-Villeurbanne, France* [q]
[54] *Pontifícia Universidade Católica do Rio de Janeiro (PUC-Rio), Rio de Janeiro, Brazil* [r]

* Corresponding author.
E-mail address: menzemer@physi.uni-heidelberg.de (S. Hansmann-Menzemer).
[a] P.N. Lebedev Physical Institute, Russian Academy of Science (LPI RAS), Moscow, Russia.
[b] Università di Bari, Bari, Italy.
[c] Università di Bologna, Bologna, Italy.
[d] Università di Cagliari, Cagliari, Italy.
[e] Università di Ferrara, Ferrara, Italy.
[f] Università di Firenze, Firenze, Italy.
[g] Università di Urbino, Urbino, Italy.
[h] Università di Modena e Reggio Emilia, Modena, Italy.
[i] Università di Genova, Genova, Italy.
[j] Università di Milano Bicocca, Milano, Italy.
[k] Università di Roma Tor Vergata, Roma, Italy.
[l] Università di Roma La Sapienza, Roma, Italy.
[m] Università della Basilicata, Potenza, Italy.
[n] LIFAELS, La Salle, Universitat Ramon Llull, Barcelona, Spain.
[o] Institució Catalana de Recerca i Estudis Avançats (ICREA), Barcelona, Spain.
[p] Hanoi University of Science, Hanoi, Viet Nam.
[q] Associated member.
[r] Associated to Universidade Federal do Rio de Janeiro (UFRJ), Rio de Janeiro, Brazil.